Kink Dynamics and Step Growth on Barium Sulfate (001): A Hydrothermal Scanning Probe Microscopy Study

ARTICLE *in* THE JOURNAL OF PHYSICAL CHEMISTRY B · JULY 2000

Impact Factor: 3.3 · DOI: 10.1021/jp0001135

4 AUTHORS, INCLUDING:

Steven R. Higgins
Wright State University
57 PUBLICATIONS **787** CITATIONS
SEE PROFILE

Carrick M Eggleston
University of Wyoming
70 PUBLICATIONS **2,159** CITATIONS
SEE PROFILE

Kink Dynamics and Step Growth on Barium Sulfate (001): A Hydrothermal Scanning Probe Microscopy Study

Steven R. Higgins,*,† Dirk Bosbach,‡ Carrick M. Eggleston,† and Kevin G. Knauss§

Department of Geology and Geophysics, University of Wyoming, Laramie, Wyoming 82071; Institut für Mineralogie, Universität Münster, Corrensstrasse 24, 48149 Münster, Germany; and Geoscience and Environmental Technology Division, Lawrence Livermore National Laboratory, Livermore, California 94550

Received: January 7, 2000; In Final Form: June 19, 2000

We have measured step growth kinetics on barium sulfate (001) as a function of step length, supersaturation, and temperature. Using a one-dimensional nucleation model, we report kink detachment coefficients for ⟨120⟩ monolayer steps of $w_- = 114$ (±14), 187 (±17), and 357 (±43) s^{-1}, at 90, 108, and 125 °C, respectively, giving an activation energy, $E_a = 0.39$ (± 0.05) eV. The kink formation energy, ϵ, was found to be 0.16 (±0.02) eV. The uncertainty in this energy is sufficient to envelop the experimentally determined kink densities, but the lack of increase in experimental kink density with increase in temperature points to kinetic limitations in the experiments. Due to the kinetic limitations of growth at kinks whether they are from diffusion or attachment, our results demonstrate that knowledge of the kink kinetics as a function of temperature is important in testing the applicability of the classical thermodynamic model to kinetic data.

I. Introduction

Predicting how, and at what rate, solids grow and dissolve under various conditions requires a thorough understanding of the fundamental surface reaction mechanisms. Scanning probe microscopy (SPM) has recently afforded observation of some of the surface processes described nearly a century ago[1] (e.g., kink/step nucleation and growth) that govern the growth and dissolution of solids. SPM has revealed complexities and subtleties of both step and kink dynamics.[2−5]

The multistep process associated with crystal growth and dissolution complicates attempts to test proposed macroscopic surface kinetic mechanisms.[6,7] In this Letter, we present, for the first time, hydrothermal SPM[8] results using step velocity data as a function of step length that can be used to model the molecular-scale kink dynamics on elementary steps. Our results lend support to a kinetic-based step growth model rather than the classical thermodynamic step growth model based on the Gibbs−Thomson relation.[9]

II. Experimental Section

We used cleaved natural barium sulfate specimens in a novel flow-cell hydrothermal SPM.[8] The relative supersaturation, σ, of the barium sulfate solutions, prepared from $Na_2SO_4 \cdot 10\ H_2O$ and $Ba(NO_3)_2$ (ionic strength = 0.001 *m* $NaNO_3$), was determined by analysis of the flow-cell effluent and thermodynamic speciation codes SUPCRT[10] and EQ3/6,[11] where

$$\sigma = \ln\left(\frac{Q}{K_{sp}}\right) = \ln\left(\frac{a_{Ba^{2+}} a_{SO_4^{2}}}{K_{sp}}\right) \quad (1)$$

K_{sp} is the solubility product for barium sulfate, and a_i are the ion activities. In the speciation calculation, we have assumed $c_{Ba^{2+}} = c_{SO_4^{2-}}$, where c_i denotes concentration. Measurements of step position, and where applicable, step length, as functions of time were used to determine linear step velocities.

III. Results and Discussion

For the range of supersaturation conditions we used, barium sulfate grew by the spiral growth mechanism. Due to the 2_1 screw axis of the *Pnma* space group (aligned parallel to [001]) of barite, the two-dimensional structure of adjacent monolayers on (001) are related by a 2-fold rotation parallel to [001]. Figure 1a shows the two monolayers as they comprise the initial turn of a growth spiral. At room temperature, monolayer sector-shaped islands grow ∼10 times faster along a normal to the sector edge when compared to the velocity normal to the ⟨120⟩ straight edges (see Figure 1b).[12,13] For a given monolayer, half of the spiral turn consists of two straight ⟨120⟩ step edges whereas the other half is composed of the curved sector edge. The faster growing edges of monolayer A (Figure 1b) meet the slower growing edges in monolayer B, forming bilayer steps (see Figure 1a).

The normal velocity R of a surface growing via the spiral mechanism is

$$R = vp = \omega h \quad (2)$$

where ω is the spiral rotation frequency (Hz), v is the lateral (step) velocity, p is the resultant hillock slope, and h is the component of the Burgers vector normal to the surface. Here we focus our attention on the factors controlling ω. Through analysis of images like that in Figure 1a, we have constructed step velocity vs step length ($v(l)$ vs l) plots (e.g., Figure 2).

The theory of Burton, Cabrera, and Frank (BCF)[9] predicts that the slope, p, of a spiral hillock will be determined primarily by r_c, the radius of a critical two-dimensional nucleus in equilibrium with its surroundings, when $r_c \gg (2/19)L$ according to

$$p = \frac{mh}{19r_c + 2L} \quad (3)$$

* Corresponding author. Fax: 1-307-766-6679. E-mail: shiggins@uwyo.edu.
† University of Wyoming.
‡ Universität Münster.
§ Lawrence Livermore National Laboratory.

10.1021/jp0001135 CCC: $19.00
Published on Web 07/08/2000

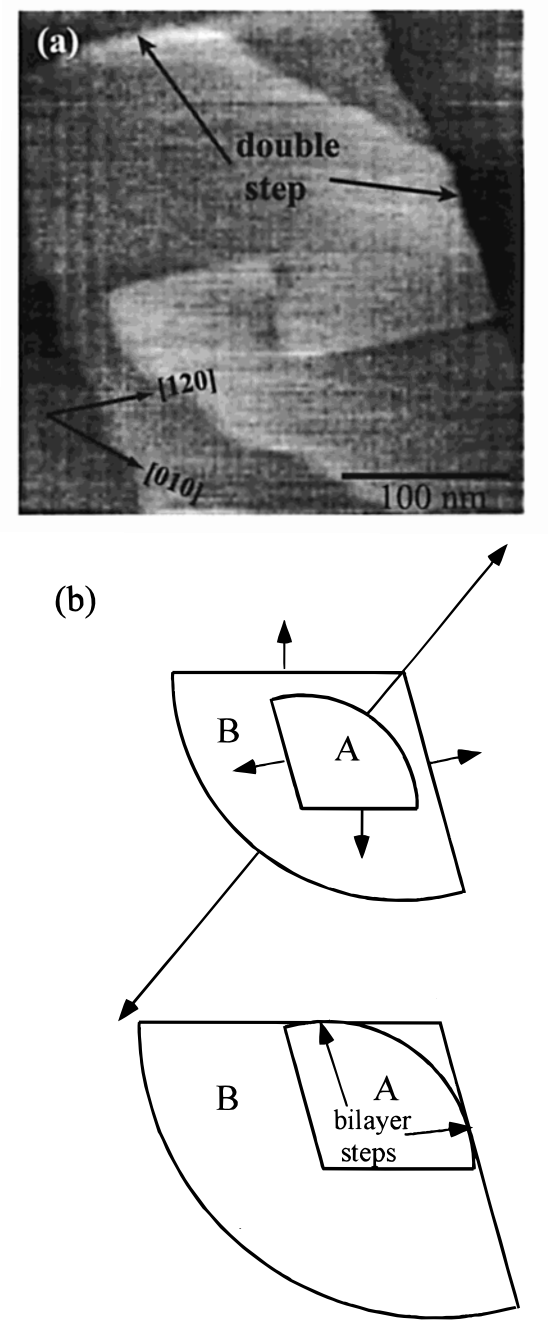

Figure 1. (a) 300 nm × 300 nm AFM image taken at 125 °C and $\sigma = 0.59$. Arrows point to the bilayer ⟨120⟩ steps. (b) Diagram of two adjacent monolayer islands showing the relationship between step orientation and relative growth velocity (indicated by length of arrows).

where L is the perimeter length, or circumference of a hollow core, encompassing all spiral sources contributing to the hillock, and m is the number of elementary steps in the Burgers vector component normal to the surface.

Equation 3 is verified via numerical methods[14] based on the assumption that some critical step radius of curvature r_c (or length, l_c, for polygonized hillocks) exists in local equilibrium with its surroundings such that the growth velocity of a step of radius r_c (length l_c) is zero (i.e., $v(l_c) = 0$). The detailed functional form of $v(l)$ in such a case is[9,15]

$$v(l) = v_\infty \frac{e^{\sigma} - e^{\sigma i_c/l}}{e^{\sigma} - 1} \tag{4}$$

so long as $l_c > \lambda_s$, an inequality that may not hold for small l_c,

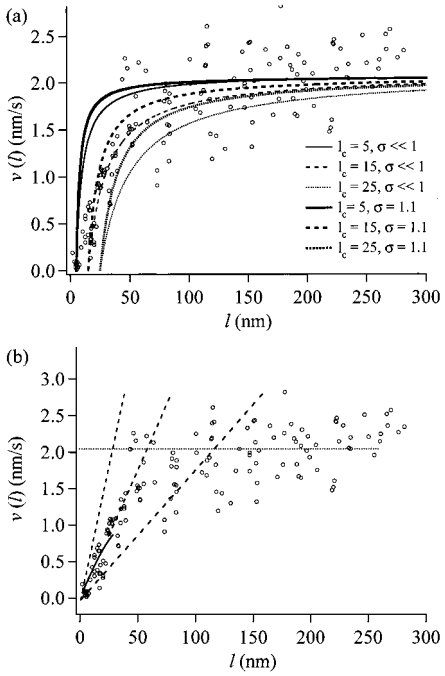

Figure 2. Velocity of steps as a function of step length at $T = 108$ °C, $\sigma = 1.1$. (a) Fitting via eq 4 does not account well for the observed behavior at $l < 100$ nm even if σ is varied. (b) The solid line is a fit to eq 5. The three dashed lines are (center dashed line) an extrapolation of the fitted solid line, and (remaining dashed lines) slopes of twice and one-half of the center dashed line. The dotted horizontal line corresponds to v_∞.

where λ_s is the mean surface diffusion length and v_∞ is the limiting step velocity at large l. Our data (e.g., Figure 2a) do not fit eq 4 well. Choosing $l_c = 15$ nm appears to fit the data best overall; however, the predicted rise in step velocity leads the observed rise in the range $l = 20-50$ nm and possibly lags the observed rise in the range $l < 20$ nm. It is likely that the observations made at $l < 20$ nm are limited in accuracy due to the radius of the AFM tip. However, truncation of all nonzero velocity data points to zero in the range $l < 15$ nm would introduce systematic bias and forces the assumption $l_c = 15$ nm. Application of eq 3 requires that the steps be in equilibrium with the surroundings.[9] If we were to apply eq 3 to the conditions at which Figure 2 was obtained with $p = 5.9 \times 10^{-3}$, $L = 0$, and replacing $19r_c$ with either $9.6l_c$ or $4l_c$ and ignoring the slight geometric correction,[15] we find $l_c = 12$ nm (using $9.6l_c$), or $l_c = 30$ nm (using $4l_c$). The data in Figure 2a imply $l_c < 5-20$ nm which is the specified AFM tip radius. Because l_c is not measurable in our data, we approach the length dependence of ⟨120⟩ monolayer step velocity in light of the kinetics of growth unit (e.g., one-dimensional "nuclei") attachment.[16−21]

Lauritzen[22] and Frank[23] developed a kinematic treatment of growth on a one-dimensional front (e.g., a step edge). The model considers a step of length l nm whose only means of advance is through formation of nuclei of depth b nm at a rate of R_{kk} nm^{-1} s^{-1} and the lateral motion of the kinks thus formed at a rate of R_k nm s^{-1}. The analytic solution gives two regions for growth. Region I is a nucleation-controlled growth regime where the step velocity is

$$v(l) = bR_{kk}l - \frac{bR_{kk}^{\,2}l^3}{3R_k} + ... \tag{5}$$

As long as the average number of kinks on the step is small (n_k

$\ll 1$), the second term in eq 5 may be neglected. [Frank[23] shows that the dimensionless quantity $P = l(R_{kk}/2R_k)^{1/2}$ must be less than about 0.1 for $v = bR_{kk}l$ to be a valid approximation to within 1%. For eq 5, $P \sim n_k/2$, or $n_k \leq 0.2$.] A description of growth in this region includes the nucleation of one growth unit on a kinkless step edge followed by growth at the two opposing kinks to the corresponding ends of the step—all occurring before the next nucleation event occurs.

Region II is a length-independent growth regime where the step contains, on average, a constant density of kinks whose value is determined by the balance between nucleation and annihilation (i.e., two kinks impact one another) events. If the number of kinks in the step is large ($n_k \gg 1$), the step velocity becomes

$$v_\infty \approx b(2R_{kk}R_k)^{1/2} \tag{6}$$

We fit eq 5 (e.g., Figure 2b) with an upper limit of l such that $v(l)/v_\infty \cong l(R_{kk}/2R_k)^{1/2} \cong 0.5$, where only the first term in v is retained.

If the above kink kinematic model is useful for describing step advance, then an appropriate combination of rate expressions for kink formation and growth kinetics ought to predict an effective rate coefficient for step advance. Following eq 6, we use the following rate expressions for the kink processes:[20,21,24,25]

$$R_k = bw_-(S - 1) \tag{7}$$

$$R_{kk} = \frac{2w_-}{b}S(S-1)e^{-2\epsilon/kT} \tag{8}$$

where w_- is the detachment frequency at kinks, ϵ is the kink formation energy, and S is the saturation state as defined below in eq 11. Implicit in the use of eqs 7 and 8 is the assumption that the forward deposition rate of Ba^{2+} is approximately equal to the forward deposition rate of SO_4^{2-} such that neither deposition process is exclusively rate-limiting.[26]

Using eqs 6−8 above, and eq 9 below

$$v = b\rho_k R_k \tag{9}$$

the kink density ρ_k as a function of supersaturation can be found using $b = 0.70$ nm:

$$\rho_k = \frac{2}{b}S^{1/2}e^{-\epsilon/kT} \tag{10}$$

Figure 3 shows (a) R_k vs $(S - 1)$ and (b) R_{kk} vs $S(S - 1)$ plots derived from the fitting procedure and (c) is a plot of $\rho_k = (2R_{kk}/R_k)^{1/2}$ (i.e., the mean kink density) vs $S^{1/2}$, where

$$S \equiv \left(\frac{a_{Ba^{2+}}a_{SO_4^{2-}}}{K_{sp}}\right)^{1/2} \approx \frac{a_{Ba^{2+}}}{\sqrt{K_{sp}}} \tag{11}$$

The value of R_k is a composite measure along the ⟨120⟩ steps because opposing kinks on this step are structurally inequivalent. The trend in Figure 3c suggests that the step roughens with increasing S. This trend is consistent with the hypothesis that kinetics control the rate of step advance because ρ_k is not expected to vary with S for steps in equilibrium.[9] Burton et al.[9] predict that for homopolar crystals, the equilibrium kink spacing is on the order of ~4 lattice spacings. This prediction either indicates that a kinetic treatment is invalid here or that the energy associated with kink formation along the ⟨120⟩ steps is higher than estimated for nonionic materials. The latter can be justified through electrostatic potential energy contributions to the kink energy, which will be larger in an ionic crystal (e.g., Pina et al.[12]). Through these arguments, we believe that for the temperatures employed in our study, the population of kink sites along the straight ⟨120⟩ monolayer steps is governed not by equilibrium thermal excitation/exchange, but by nonequilibrium *processes* giving rise to step motion.

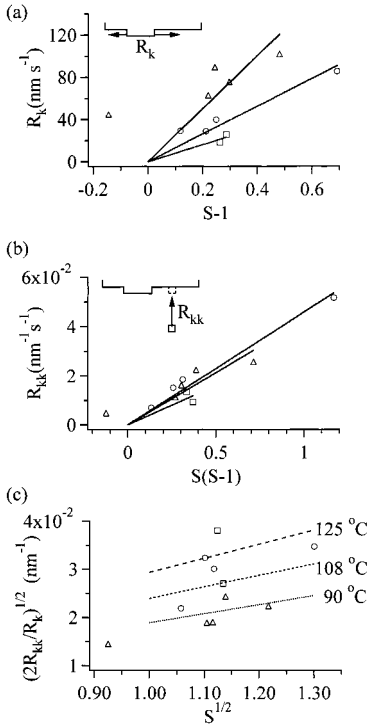

Figure 3. (a) R_k vs $(S - 1)$; (b) R_{kk} vs $S(S - 1)$ plots derived from the fitting procedure; and (c) a plot of $\rho_k = (2R_{kk}/R_k)^{1/2}$ (i.e., the mean kink density) vs $S^{1/2}$. Squares 90 °C; circles 108 °C; triangles 125 °C.

TABLE 1: Experimental Values for the Kink Detachment Frequencies, Activation Energy, Kink Formation Energy, and Kink Kinetic Coefficients[a]

temp (°C)	w_- (s^{-1})	ϵ (eV)	$\beta_k \approx \beta_{st}$ (cm s^{-1}) (predicted)
90	114 (±14)	0.14 (± 0.01)	9 (±2)
108	187 (±17)	0.15 (± 0.01)	15 (±2)
125	357 (±43)	0.17 (± 0.01)	30 (±3)
	$E_a = 0.39$ (±0.05) eV	$\bar{\epsilon} = 0.16$ (± 0.02)	

[a] The predicted step kinetic coefficients, β_{st}, were obtained in the rough step limit.

We fit our data in Figure 3, a and b, to eqs 7 and 8, to determine w_- and ϵ (see Table 1), respectively.[20] Following Chernov et al.,[27] we can determine the *kink* kinetic coefficient, β_k, by eq 12:

$$\beta_k = \frac{bw_-}{a_{eq}\Omega} \tag{12}$$

where a_{eq} is the activity of molecules at equilibrium and Ω is the crystal molar volume. Furthermore, as the step approaches the roughened limit at high supersaturation, $\beta_{st} \approx \beta_k$, where β_{st} is the step kinetic coefficient (see Table 1).

Questions raised by a referee led us to consider how the thermodynamic prediction of a critical length, or critical size, is not violated on the basis of a one-dimensional nucleation process. Zhang and Nancollas[26] stated the issue of whether one-dimensional nucleation occurs or not as a matter of criteria for

nucleation. They argue that if a critical size must be reached in order for there to be one-dimensional nucleation, then one-dimensional nucleation is not possible on the steps. We add that thermodynamics would never allow a single unit to grow unless the critical size was that of a single unit. However, if the nucleation process only occurs when a one-dimensional cluster reaches a length where it is *more likely than not* to survive, then the attachment of one growth unit to the step may be considered as one-dimensional nucleation so long as the unit is still *more likely than not* to detach before it reaches the critical size. This does not violate the predicted existence of a thermodynamic critical size.

If diffusion on the surface and/or along the edge is not sufficiently rapid to maintain equilibrium everywhere along the step, then the resultant kinetically limited critical size will necessarily be longer than the thermodynamic critical size in the case of infinitely fast diffusion.[21] In other words, for a diffusion limitation, only the kinks remain in equilibrium, but S then rises between neighboring kinks and, as a result, the removal by detachment of the cluster is opposed by the kinkless regions of higher S. How large an overestimate in the thermodynamic critical size is obtained for a transport-impeded process is difficult to determine if equilibrium at steps cannot be assumed.

Using eqs 6−8, we obtain a rate expression for v_∞ that depends on the supersaturation S:[20]

$$v_\infty = 2bw_-(S-1)S^{1/2}e^{-\epsilon/kT} \tag{13}$$

where w_- has an Arrhenius form

$$w_- = w_0 e^{-E_a/RT} \tag{14}$$

and E_a is the activation barrier to desorption from a kink site and will contain all barriers including diffusional components. Although eq 13 does not predict the linear relationship between v_∞ and S so often found in the literature,[28−32] our step velocity data displayed a superlinear dependence on S. Voronkov and Rashkovich[33] developed an impurity-based model to explain this superlinear dependence, but the superlinear behavior can also be explained by kinetic roughening of the step.[34,35] The step velocity in eq 13 is superlinear in S because at low S, both ρ_k and R_k increase (see eq 9) with S until ρ_k reaches the rough step limit. The idea of kinetic roughening is supported by our data (Figure 3(c)).

Figure 4a shows the step velocities for the ⟨120⟩ bilayer steps, as a function of $S^{1/2}(S-1)$. The slopes of the lines in Figure 4a should follow Arrhenius behavior giving an effective activation energy, $E_{a(eff)} = E_a + \epsilon$. Using $\bar{\epsilon}$ (Table 1), the slopes of the lines in Figure 4b give $E_a = 0.39 \pm 0.05$ and 0.30 ± 0.05 eV for the predicted and measured step velocity data (Figure 4a), respectively. These numbers are questionable in terms of being statistically similar and suggest a transport limit to the flux at steps, particularly at 125 °C.

Regarding possible mass transport limits on the observed kinetics at 125 °C, we determined the rate of motion of a step bunch with a slope $p = 0.012$ relative to a growth hillock with a slope $p = 0.0035$. The step velocity within the higher sloped bunch, $v(p{=}0.012)$, was indistinguishable from $v(p{=}0.0035)$. In a bulk diffusion-controlled process where the diffusion layer thickness, $\delta \gg y_0 \equiv h/p$, the step velocity is proportional to y_0 (step spacing)[36,37] which is not consistent with our observations. As $\delta \sim y_0$, surface diffusion theories[38,39] must be considered. In this model, as long as $y_0 > 6\lambda_s$, v_∞ should be independent of

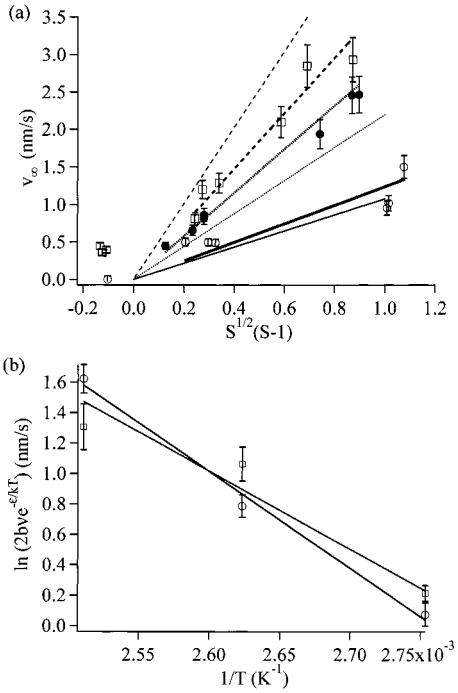

Figure 4. (a) Plot of step velocity versus $S^{1/2}(S-1)$ at 90 °C (open circles), 108 °C (closed circles), and 125 °C (open squares). Thick lines are fitted to eq 13 and thin lines are based on the parameters obtained from Figure 3. (b) Arrhenius plot of the slope of the lines in (a) versus temperature, $\ln(2bv\exp(-\epsilon/kT))$ vs $1/T$. The squares represent the fitted slopes and the circles represent the slopes corresponding to the parameters obtained from Figure 3.

y_0. At this point, we can only estimate that $\lambda_s < y_0$, or ∼60 nm using the value of y_0 for the step bunch.

Surface diffusion could explain the lack of Arrhenius behavior for R_{kk}, and thus ρ_k. For $\lambda_s \sim \rho_0^{-1}$, the mean S at the step will be a function of ρ_0, the equilibrium kink density.[9] Increasing temperature with constant S in the bulk, which should decrease both λ_s and ρ_0^{-1}, will likely reduce S near the steps. The quantity $\lambda\rho_0^{-1}$ should increase with temperature[9] and at high temperature, equilibrium is established everywhere along the step. Poor fluid transport control near the surface may be problematic in assuming a value of S on the surface, an issue recently addressed quantitatively in AFM studies of heterogeneous kinetics.[40,41] A second systematic underestimate in R_{kk} could arise if the AFM temporal/spatial response function is not adequate to follow the true rise in step velocity with length. The temporal error is significant if the image period is only $^1/_4$−$^1/_2$ times the period required for $v(l) \sim v_\infty$. An overestimate of R_{kk} will generally result due to length errors because at small l, the tip radius will make the *apparent* l greater than the *actual* l. These two errors tend to offset one another and are not likely to be significant in our evaluation.

We return briefly to the discussion regarding l_c which we estimated to be between 12 and 30 nm using eq 3 under conditions identical to those of Figure 2. This leads to estimates for the edge free energy, γ, ranging from 0.31 to 0.77 eV/site. For high γ values ($\gamma \gg kT$), $\gamma \sim \epsilon$ [42] and lead to $\rho_0^{-1} \approx 12\ \mu$m to 20 m! These spacings are not reasonable and lead to doubt in the approximation $\gamma \sim \epsilon$. However, it is easy to overestimate l_c at small l and if transport plays a role between kinks, then the assumptions of the equilibrium model are invalid. Both errors could account for a 50% overestimate in γ which results in large errors in ρ_0 even if $\gamma \sim \epsilon$ is valid.

The kink-limited step growth model of Voronkov[34] may also be applied here for comparison. This model is valid if the kink

spacing $\rho_k^{-1} > 5l_c$. If $\rho_k^{-1} \gg l_c$, then the approximation below is reasonable:

$$\rho_k^{-1} \approx \frac{e y_0}{8} \tag{15}$$

For the Figure 2 data ($y_0 = 120$ nm), we obtain $\rho_k = 2.5 \times 10^{-2}$ nm^{-1} which leads to $\epsilon = 0.16$ eV. This value agrees well with the kink kinetic prediction of $\epsilon = 0.16$ (± 0.02) eV. This agreement, however, should be expected as Voronkov's model is equivalent to the above kink kinetic treatment if $\rho_k^{-1} \gg l_c$ is valid. The step velocity in this model should rise from $v(l) = 0$ to v_∞ over a distance $\Delta l = 2\rho_k^{-1}$ which for $y_0 = 120$ nm would mean $\Delta l = 80$ nm. The step velocity in Figure 2 rises to v_∞ over $\Delta l \approx 100$ nm which is reasonably close within error and supports the validity of the assumptions in eq 15. The kinetic approach, in light of the models considered, offers an alternative to the usual equilibrium step model for obtaining an experimental value for ϵ.

IV. Summary

Through detailed determination of the step kinetics on barium sulfate (001), we have described the ⟨120⟩ straight monolayer step advance by means of a one-dimensional nucleation model. Through this model, we have determined kink detachment frequencies and the activation energy of the detachment process. We also determined the kink formation energy to be 0.16 (± 0.02) eV. Because surface diffusion could not be excluded, the kink kinetics likely contain a diffusional component, and thus, are only apparent quantities. We conclude that a kinetic model more appropriately describes step advance under conditions where l_c is small and ϵ moderate, giving rise to the possibility that the steps do not maintain equilibrium with the immediate surroundings on the time scale of kink attachment/detachment events.

Acknowledgment. The authors acknowledge the curators of the Cambridge University mineral repository for donation of the barite specimens, Dr. James DeYoreo of Lawrence Livermore National Laboratory for his many helpful comments during the revision process, the U.S. Department of Energy, Office of Basic Energy Sciences (KC040302 to K.G.K., DE-FG03-96SF14623 to C.M.E.), the National Science Foundation (EAR-9634143 to C.M.E.), and the Deutsche Forschungsgemeinschaft (D.B.) for financial support.

References and Notes

(1) Stranski, I. N. *Z. Phys. Chem.* **1928**, *136*, 259.
(2) Jordan, G.; Rammensee, W. *Geochim. Cosmochim. Acta* **1996**, *60*, 5055.
(3) Kuznetsov, Y. G.; Malkin, A. J.; McPherson, A. *J. Cryst. Growth* **1999**, *196*, 489.
(4) Land, T. A.; Malkin, A. J.; Kuznetsov, Y. G.; McPherson, A.; DeYoreo, J. J. *Phys. Rev. Lett.* **1995**, *75*, 2774.
(5) Bosbach, D.; Junta-Rosso, J. L.; Becker, U.; Hochella, M. F. *Geochim. Cosmochim. Acta* **1996**, *60*, 3295.
(6) Compton, R. G.; Unwin, P. R. *Philos. Trans. R. Soc. London A* **1990**, *330*, 1.
(7) Unwin, P. R.; Barwise, A. J.; Compton, R. G. *J. Colloid Interface Sci.* **1989**, *128*, 208.
(8) Higgins, S. R.; Eggleston, C. M.; Knauss, K. G.; Boro, C. O. *Rev. Sci. Instrum.* **1998**, *69*, 2994.
(9) Burton, W. K.; Cabrera, N.; Frank, F. C. *Philos. Trans. R. Soc. London* **1951**, *A243*, 299.
(10) Johnson, J. W.; Oelkers, E. H.; Helgeson, H. C. *Comput. Geosci.* **1992**, *18*, 899.
(11) Wolery, T. J.; Jackson, K. J.; Bourcier, W. L.; Bruton, C. J.; Viani, B. E.; Knauss, K. G.; Delany, J. M. The EQ3/6 software package for geochemical modeling: Current Status. In *Chemical Modeling in Aqueous Systems II*; Melchior, D. C., Bassett, R. L., Eds.; American Chemical Society: Washington, DC, 1990; Vol. 416, p 104.
(12) Pina, C. M.; Becker, U.; Risthaus, P.; Bosbach, D.; Putnis, A. *Nature* **1998**, *395*, 483.
(13) Bosbach, D.; Hall, C.; Putnis, A. *Chem. Geol.* **1998**, *151*, 143.
(14) Budevski, E.; Staikov, G.; Bostanov, V. *J. Cryst. Growth* **1975**, *29*, 316.
(15) Teng, H. H.; Dove, P. M.; Orme, C. A.; DeYoreo, J. J. *Science* **1998**, *282*, 724.
(16) Liang, Y.; Baer, D. R. *Surf. Sci.* **1997**, *373*, 275.
(17) McCoy, J. M.; LaFemina, J. P. *Surf. Sci.* **1997**, *373*, 288.
(18) Chernov, A. A. *Mater. Sci. Forum* **1998**, *276−277*, 71.
(19) Gates, D. J.; Westcott, M. *J. Stat. Phys.* **1994**, *77*, 199.
(20) Zhang, J.; Nancollas, G. H. *J. Cryst. Growth* **1990**, *106*, 181.
(21) Temkin, D. E. *Sov. Phys. Crystallogr.* **1969**, *14*, 179.
(22) Lauritzen, J. I. *J. Appl. Phys.* **1973**, *44*, 4353.
(23) Frank, F. C. *J. Cryst. Growth* **1974**, *22*, 233.
(24) Voronkov, V. V. *Sov. Phys. Crystallogr.* **1968**, *13*, 13.
(25) Voronkov, V. V. *Sov. Phys. Crystallogr.* **1970**, *15*, 8.
(26) Zhang, J.; Nancollas, G. H. *J. Colloid Interface Sci.* **1998**, *200*, 131.
(27) Chernov, A. A.; Rashkovich, L. N.; Yaminski, I. V.; Gvozdev, N. V. *J. Phys. Condens. Matter* **1999**, *11*, 9969.
(28) Maiwa, K.; Tsukamoto, K.; Sunagawa, I. *J. Cryst. Growth* **1990**, *102*, 43.
(29) Malkin, A. J.; Kuznetsov, Y. G.; Glantz, W.; McPherson, A. *J. Phys. Chem.* **1996**, *100*, 11736.
(30) Land, T. A.; DeYoreo, J. J.; Lee, J. D. *Surf. Sci.* **1997**, *384*, 136.
(31) Rashkovich, L. N. *KDP Family of Single Crystals*; Adam-Hilger: New York, 1991.
(32) Teng, H. H.; Dove, P. M.; DeYoreo, J. J. *Geochim. Cosmochim. Acta* **1999**, *63*, 2507.
(33) Voronkov, V. V.; Rashkovich, L. N. *J. Cryst. Growth* **1994**, *144*, 107.
(34) Voronkov, V. V. *Sov. Phys. Crystallogr.* **1973**, *18*, 19.
(35) DeYoreo, J. J., manuscript in preparation.
(36) Frank, F. C. On the Kinematic Theory of Crystal Growth and Dissolution Processes. In *Growth and Perfection of Crystals*; Doremus, R. H., Roberts, B. W., Turnbull, D., Eds.; Wiley: New York, 1958.
(37) Sangwal, K. *Etching of Crystals. Theory, Experiment, and Application*; North-Holland: Amsterdam, 1987.
(38) Hirth, J. P.; Pound, G. M. *J. Chem. Phys.* **1957**, *26*, 1216.
(39) Gilmer, G. H.; Ghez, R.; Cabrera, N. *J. Cryst. Growth* **1971**, *8*, 79.
(40) Coles, B. A.; Compton, R. G.; Booth, J.; Hong, Q.; Sanders, G. H. W. *J. Chem. Soc., Chem. Commun.* **1997**, 619.
(41) Coles, B. A.; Compton, R. G.; Suárez, M.; Booth, J.; Hong, Q.; Sanders, G. H. W. *Langmuir* **1998**, *14*, 218.
(42) Zhang, J.-W.; Nancollas, G. H. Mechanisms of growth and dissolution of sparingly soluble salts. In *Mineral-Water Interface Geochemistry*; Hochella, M. F., White, A. F., Eds.; Mineralogical Society of America: Washington, 1990; Vol. 23.